Applied Physics Letters

RESEARCH ARTICLE | NOVEMBER 28 2023

Bi_2Se_3 interlayer treatments affecting the $Y_3Fe_5O_{12}$ (YIG) platinum spin Seebeck effect

Yaoyang Hu ; Michael P. Weir ; H. Jessica Pereira ; Oliver J. Amin ; Jem Pitcairn ; Matthew J. Cliffe ; Andrew W. Rushforth ; Gunta Kunakova ; Kiryl Niherysh ; Vladimir Korolkov; James Kertfoot; Oleg Makarovsky ; Simon Woodward

Appl. Phys. Lett. 123, 223902 (2023)
https://doi.org/10.1063/5.0157778

Applied Physics Letters ARTICLE pubs.aip.org/aip/apl

Bi_2Se_3 interlayer treatments affecting the $Y_3Fe_5O_{12}$ (YIG) platinum spin Seebeck effect

Cite as: Appl. Phys. Lett. **123**, 223902 (2023); doi: 10.1063/5.0157778
Submitted: 11 May 2023 · Accepted: 2 November 2023 ·
Published Online: 28 November 2023

View Online Export Citation CrossMark

Yaoyang Hu,[1,a)] Michael P. Weir,[2,a)] H. Jessica Pereira,[1,3] Oliver J. Amin,[2] Jem Pitcairn,[4] Matthew J. Cliffe,[4] Andrew W. Rushforth,[2] Gunta Kunakova,[5] Kiryl Niherysh,[5] Vladimir Korolkov,[6,b)] James Kertfoot,[6,b)] Oleg Makarovsky,[2] and Simon Woodward[1]

AFFILIATIONS

[1]GSK Carbon Neutral Laboratories for Sustainable Chemistry, University of Nottingham, Jubilee Campus, Nottingham NG7 2TU, United Kingdom
[2]School of Physics and Astronomy, University of Nottingham, Nottingham NG7 2RD, United Kingdom
[3]School of Electronics and Computer Science, University of Southampton, Southampton SO17 1BJ, United Kingdom
[4]School of Chemistry, University of Nottingham, University Park Campus, Nottingham NG7 2RD, United Kingdom
[5]Institute of Chemical Physics, University of Latvia, LV-1586 Riga, Latvia
[6]Park Systems UK Limited, MediCity Nottingham, Thane Road, Nottingham NG90 6BH, United Kingdom

[a)]Authors to whom correspondence should be addressed: yaoyanghuchem@gmail.com; and michael.weir@nottingham.ac.uk
[b)]URL: pse@parksystems.com

ABSTRACT

In this work, we present a method to enhance the longitudinal spin Seebeck effect at platinum/yttrium iron garnet (Pt/YIG) interfaces. The introduction of a partial interlayer of bismuth selenide (Bi_2Se_3, 2.5% surface coverage) interfaces significantly increases (by ~380%–690%) the spin Seebeck coefficient over equivalent Pt/YIG control devices. Optimal devices are prepared by transferring Bi_2Se_3 nanoribbons, prepared under anaerobic conditions, onto the YIG (111) chips followed by rapid over-coating with Pt. The deposited Pt/Bi_2Se_3 nanoribbon/YIG assembly is characterized by scanning electron microscope. The expected elemental compositions of Bi_2Se_3 and YIG are confirmed by energy dispersive x-ray analysis. A spin Seebeck coefficient of 0.34–0.62 μV/K for Pt/Bi_2Se_3/YIG is attained for our devices, compared to just 0.09 μV/K for Pt/YIG controls at a 12 K thermal gradient and a magnetic field swept from -50 to $+50$ mT. Superconducting quantum interference device magnetometer studies indicate that the magnetic moment of Pt/Bi_2Se_3/YIG treated chips is increased by ~4% vs control Pt/YIG chips (i.e., a significant increase vs the $\pm$0.06% chip mass reproducibility). Increased surface magnetization is also detected in magnetic force microscope studies of Pt/Bi_2Se_3/YIG, suggesting that the enhancement of spin injection is associated with the presence of Bi_2Se_3 nanoribbons.

Spin Seebeck effects (SSE) arise from spin current (magnon) generation from within ferri-, ferro-, or anti-ferromagnetic materials driven by an applied temperature gradient.[1] Longitudinal spin Seebeck effect (LSSE) investigations, where the spin current and temperature gradient evolve along a common z axis, while the magnetic field is applied in the y axis and the voltage contacts are spaced along the x axis [Fig. 1(a)], have become the most popular spin Seebeck device architecture.[2,3] While this configuration minimizes any anomalous or planar Nernst voltage effects from the magnetic layer,[4,5] it also requires the use of an insulating magnetic material. Typically, therefore, this role is fulfilled by crystalline yttrium iron garnet ($Y_3Fe_5O_{12}$, YIG) grown on the (111) plane of a gadolinium gallium garnet (GGG) substrate. Direct detection of YIG-derived spin currents is presently challenging, so a metallic layer with a large spin–orbit coupling (typically platinum) is placed on top of the YIG to convert the spin current into a voltage (V_{LSSE}) via the inverse spin Hall effect (ISHE).[6,7] The spin mixing conductance characterizes the transport efficiency of spin current through the interface (e.g., Pt/YIG)[8] and should be maximized for these applications. Silver/YIG has also been proposed as an alternative to Pt/YIG and investigated theoretically, showing a high spin mixing conductance.[9] Theoretically, the SSE could form the basis of future

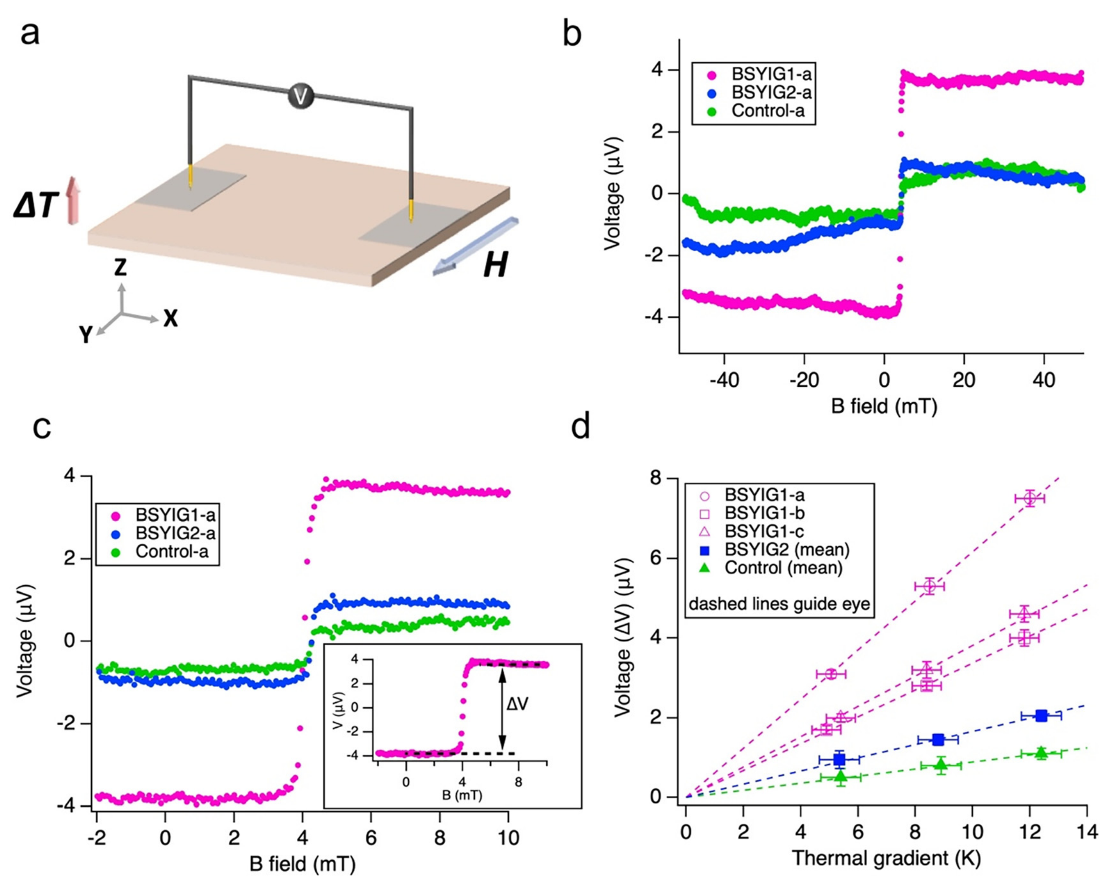

FIG. 1. (a) Graphical illustration of the LSSE device under a magnetic field ***H*** and thermal gradient ΔT. The device consists of Pt coated on YIG, with two areas of $0.5 \times 2\,mm^2$ silver paste as the contacts to the probes. (b) Example LSSE measurements with thermal gradient at 12 K and magnetic field sweep from −50 to +50 mT: Pt on un-oxidized Bi_2Se_3 flakes on YIG (**BSYIG1-a**, pink), Pt on aerobically oxidized Bi_2Se_3 flakes on YIG (**BSYIG2-a**, blue) and a control sample (**Control-a** Pt on YIG, green). (c) LSSE measurements in the region of interest around the voltage change (−2 to +10 mT). **Inset:** illustration of the extraction of ΔV (V_{LSSE}) from the V vs B data. (d) ΔV (V_{LSSE}) vs ΔT with thermal gradient at ∼5, 8, and 12 K for **BSYIG1-a, BSYIG1-b, BSYIG1-c, BSYIG2 (mean)**, and **Control (mean)** including linear fits to the data extrapolated to ΔT, $\Delta V = 0$.

spin-caloritronic sustainable heat energy recovery technologies.[10] Presently, however, significant practical difficulties need to be overcome before delivering such outcomes. One important issue is that in most published SSE investigations, using devices of dimensions typically of the order of $1\,cm^2$, reported values of V_{LSSE} lie only in the range up to a few microvolts (μV).[2,3] While only thin layers of YIG (ca. 0.1–500 μm) and Pt (ca. 5 nm) are required for SSE generation, the fabrication of large area bi-layer Pt/YIG devices can become non-viable, even if such architectures are stacked. One potential solution would be to place an additional spintronic material at the YIG-Pt interface that is able to improve the ISHE dramatically, generating higher V_{LSSE} values and ultimately more power. Chemical treatments of the top of the YIG interface itself might also be used to attain this enhanced ISHE. Comprehensive theoretical models linking the structure of the YIG surface with spin current recombination are largely lacking, and, thus, the understanding of how such additional layers and treatment effects can promote enhanced ISHE is still in its infancy and mainly driven by experiment. A wide range of interlayers have been studied,[1,11–15] and their presence has been observed to produce a wide variety of effects, including (a) no effect on the V_{LSSE}, as in the use of gold interlayers and piranha treated YIG,[16] (b) negative effects, such as those of magnetic insulators (e.g., $SrTiO_3$), where the V_{LSSE} is *reduced* by a factor of >100,[17] and (c) enhancement of the SSE. A few significant examples of SSE enhancements are as follows: (i) the use of a C_{60} interlayer ($V_{LSSE} = 95$ nV/K with 5 nm C_{60}, 5 nm Pt at 300 K; control $V_{LSSE} = 55$ nV/K in the absence of C_{60});[18] (ii) the use of WSe_2 flakes ($V_{LSSE} = 7.1\,\mu$V/K with 0.9 nm WSe_2 at unspecified coverage, 5 nm Pt at 300 K; control $V_{LSSE} = 2.2\,\mu$V/K in the absence of WSe_2);[19,20] (iii) the use of MoS_2 layers ($V_{LSSE} = 1.5\,\mu$V/K with ∼15 nm MoS_2 at 40% coverage, 5 nm Pt at 300 K; control $V_{LSSE} = 0.3\,\mu$V/K in the absence of MoS_2);[21] (iv) the use of NiO layers (relative increases of ∼3.5 vs control samples at 300 K[22] as well as decreases[23] have been reported); and (v) the employment of metal alloys [Pt/$Fe_{70}Cu_{30}$ (0.3 nm)/Bi-YIG relative increase in 1.7 times vs control sample].[24] Herein, we discuss the discovery of a *significant enhancement* in the longitudinal spin Seebeck (V_{LSSE} increased by ∼380%–690%)

using Bi_2Se_3 nanoribbons. We additionally report on how generic sample preparation methods can affect spin Seebeck measurements when seeking to evaluate the performance of interface materials.

In screening for interlayer improvement materials, the thickness of the upper Pt electrode needs consideration. Due to the short spin diffusion length in platinum ($\lambda \sim$1.9 nm),[25] thin Pt layers are preferred for SSE studies. However, attaining high sample-to-sample reproducibility in the Pt layer thickness is vital in eliminating false positives when screening the effectiveness of spin Seebeck interface additives. The highest chip-to-chip reproducibility using our sputter coating setup was obtained for 18 ± 2 nm platinum coatings, and this was chosen as the coating thickness for all samples. Under such experimental conditions, only high-performing additives are detected in screening studies. Using this approach, we have identified Bi_2Se_3 nanoribbons as a high-performing YIG/Pt interface material. Similarly, we found that over-aggressive cleaning of our YIG chips could also induce slight variations in nominally identical chips. We, therefore, always used the reproducible procedure outlined in the supplementary material SI2.

Nanoribbons of Bi_2Se_3 were prepared as previously described[26] and transferred to rigorously clean, flat, and precision-cut YIG chips (5.1 μm YIG on GGG, Matesby GmbH, 5.00 × 5.00 mm^2, weight variation ≤0.06%; for more information on the samples and preparation, see the supplementary material) under an inert atmosphere, and the Bi_2Se_3 ribbons temporarily protected from air by a polymeric PMMA layer (sample type **BSYIG1**; three samples: **BSYIG1-a**, **BSYIG1-b,** and **BSYIG1-c**, where samples **b** and **c** were prepared under identical conditions to sample **a** investigate reproducibility). Nanoribbon Bi_2Se_3 is known to be susceptible to aerobic oxidation, so as a check, equivalent samples were allowed to reach the thermodynamic surface oxidized state by exposure to air for >5 days (sample type **BSYIG2**; 2 samples: **BSYIG2-a** and **BSYIG2-b**, both prepared under identical conditions). Their Bi_2Se_3 ribbon coverage (2.5%) was comparable to those samples not exposed to air. Finally, Pt/YIG chips (sample type **Control**; 2 samples, **Control-a** and **Control-b**, both prepared under identical conditions) were prepared by simple platinum coating of the same YIG chip batch (at a Pt thickness of 18 ± 2 nm). To compare surface oxidation effects for **BSYIG1** samples, the PMMA protective layers were always removed under argon immediately prior to Pt-coating. The Bi_2Se_3 surface coverage of YIG samples **BSYIG1-a/b/c** and **BSYIG2-a/b** was directly comparable (2.5%).

All Bi_2Se_3 nanoribbon tri-layer coated chips (sets **BSYIG1** and **BSYIG2**) showed enhanced spin Seebeck effects compared to the simple bi-layer Pt/YIG (**Control** set) with a temperature differential ΔT up to ~12 K (mid-point 293 K). Figure 1(b) shows an overview of the LSSE measurements for samples **BSYIG1-a**, **BSYIG2-a**, and **Control-a** across a magnetic field sweep from −50 to +50 mT, while Fig. 1(c) provides better visibility of the region around the voltage switching, in the range −2 to +10 mT (with switching in our samples typically occurring around +4 mT). The inset of Fig. 1(c) shows how the change in voltage $\Delta V = V_{LSSE}$ was derived from the sweeps of V vs B. A full review of our spin Seebeck measurement and data reduction scheme can be found in the supplementary material. The SSE enhancement is most significant for un-oxidized samples (**BSYIG1-a/b/c**) at magnetic fields of ±50 mT. Repeating SSE measurements at target values of ΔT = 5, 8, and 12 K [same mid-point, Fig. 1(d)] confirmed SSE coefficients of 0.62 ± 0.03, 0.34 ± 0.02, and 0.38 ± 0.03 μV/K for **BSYIG1-a**, **BSYIG1-b**, and **BSYIG1-c**, respectively. Samples **BSYIG2-a** and **BSYIG2-b** yielded SSE coefficients of 0.16 ± 0.02 and 0.17 ± 0.02 μV/K, respectively, while **Control-a** and **Control-b** yielded 0.08 ± 0.01 and 0.10 ± 0.01 μV/K, respectively. Since two samples each were measured for both **BSYIG2** and **Control**, for visual clarity, the mean and standard error of these measurements is shown in Fig. 1(d), with the full graph and table of values and uncertainties included in the supplementary material.

In Fig. 1(d), linear fits to the data points are provided and extrapolated to $\Delta T = 0$, assuming that $V_{LSSE} = 0$ at $\Delta T = 0$, and these lines serve to guide the eye. These lines illustrate that the spin Seebeck response is necessarily linear in all cases. Thus, anaerobically prepared Bi_2Se_3 interlayers (**BSYIG1**) lead to increases in spin Seebeck coefficient within the range 380 ± 20 to 690 ± 30% over the mean of the **Control** samples under identical conditions. To ensure that the observed enhancement is solely spintronic in origin, without contributions from traditional (thermal) Seebeck effects, we studied the device resistance for chips **BSYIG1-a**, **BSYIG2-a**, and the **Control-a** (see the supplementary material). Each of the three samples showed no variation in their intrinsic resistance (±0.1%) when subjected to the same ΔT = 5, 8, and 12 K temperature differentials, consistent with the absence of a conventional Seebeck effect. The difference in resistance between **BSYIG2-a** and the other samples (**BSYIG1-a** and **Control-a**) is attributed to the oxidization of YIG during the process of air exposure. Such resistance differences would require further consideration in the development of these materials as thermoelectric generators. However, since **BSYIG1-a** has a similar resistance to the **Control-a** Pt/YIG sample, this suggests the anaerobic insertion of Bi_2Se_3 has not had a detrimental effect.

Stochastic sampling of representative surface areas of the **BSYIG1-a** sample by scanning electron microscope (SEM) revealed the uniform presence of Bi_2Se_3 nanoribbons in SEM images (Fig. 2). The Bi_2Se_3 ribbons range (randomly) in lateral size from ca. 0.8 μm plates to extended ribbons up to 11 μm wide by 25 μm long. Image averaging (using *ImageJ*)[27] provides a coverage of 2.5 ± 1.3% for the 5.00 × 5.00 mm^2 chips. The average composition of representative nanoribbon flakes, and of the surface as a whole, was quantified with energy dispersive x-ray (EDX) (Fig. 2). The majority of the YIG surface exhibits a composition identical to native YIG (sample **Control**), while bismuth and selenium were solely detected in the nanoribbons. The appearance of the **BSYIG2-a** (aerobically oxidized) sample under SEM was not distinguishable from that of **BSYIG1-a**. Equivalent EDX data were obtained for Bi_2Se_3 flake composition between the oxidized and un-oxidized samples. The absence of a discernible oxygen signal for **BSYIG2-a** Bi_2Se_3 flakes is consistent with findings of Kunakova *et al.*, who found that aerobic oxidation only produces surface oxide layers of Bi_2O_3 and SeO_2.[26] While this substantially reduced the charge carrier density of the Bi_2Se_3 nanoribbons, the bulk of the Bi_2Se_3 material is not oxidized.[28] We propose that similar effects may account for the lower V_{LSSE} observed for **BSYIG2-a**, while its EDX spectrum remains identical to sample **BSYIG1-a**.

Given that a very significant SSE improvement was observed in the presence of only a small amount of Bi_2Se_3 in **BSYIG1-a**, we were interested to see if this was reflected in the magnetic properties of such chips. Bulk magnetization hysteresis loop (*M–H*) measurements on individual sample chips were carried out using a superconducting quantum interference device (SQUID) magnetometer (MPMS-XL, Quantum Design) at room temperature (300 K) to explore the in-

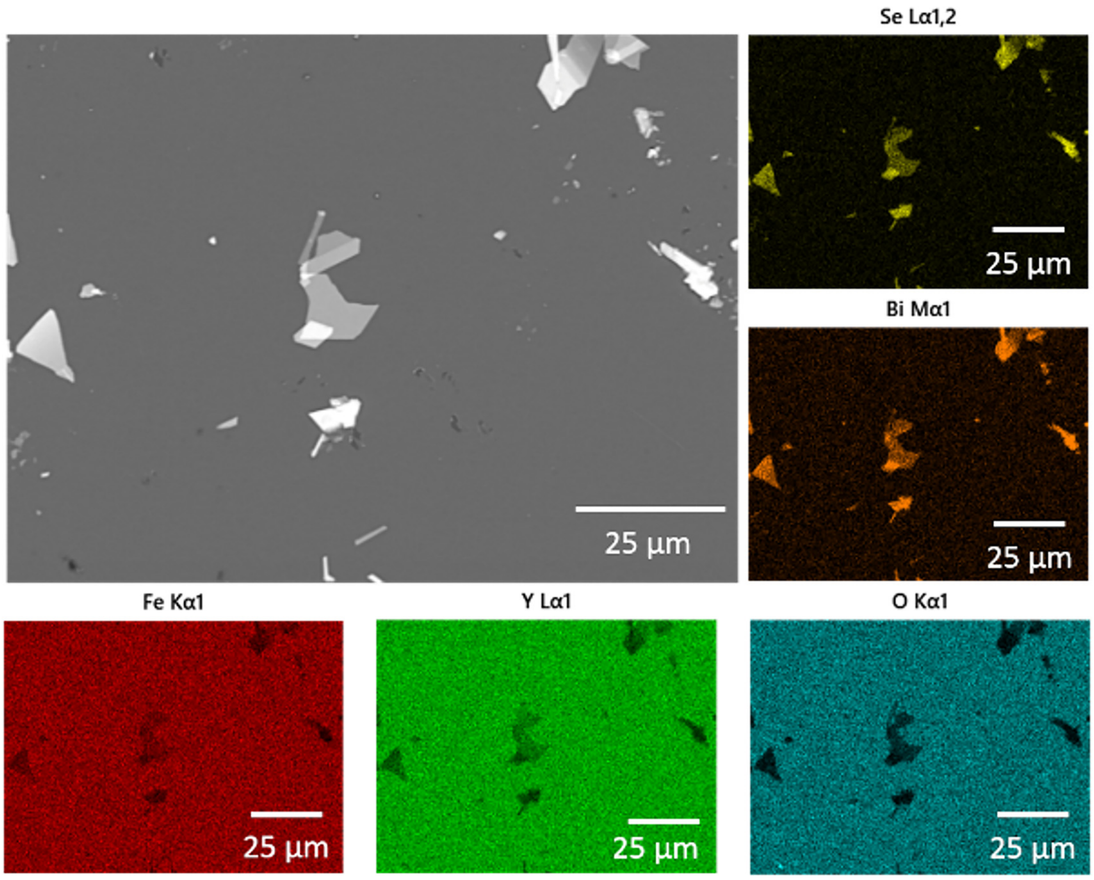

FIG. 2. SEM images (×1000 magnification) and EDX mapping of collections of Bi_2Se_3 nanostructures on YIG (**BSYIG1-a**) with EDX mapping showing the elemental composition of majority the YIG substrate. The bottom row shows maps for iron (red), yttrium (green), and oxygen (blue). Bismuth and selenium analyses of a representative single Bi_2Se_3 flake are shown to the right of the main (grey) image.

plane magnetization of Bi_2Se_3 on YIG/GGG. The measurement was initiated by stabilizing the temperature at 300 K and then sweeping the applied field from to −50 to +50 mT (see the supplementary material SI8). The behavior of **BSYIG1-a** was nearly identical to the **Control-a** Pt/YIG sample except that they showed an increased magnetization of |0.0248| emu at both −50 and +50 mT (500 Oe), over **Control-a** (|0.0236| emu), with a maximum error bar of $\leq 1.9 \times 10^{-5}$ emu. Magnetization is a mass-related property, but control experiments confirmed a consistent mass for our precision-cut YIG chips (weighed to 0.000 05 mg accuracy), which was reproducible to within ±0.06% (across a set of samples including as-supplied un-coated wafers and **BSYIG1-a/b/c**). The magnetism observed for the **BSYIG1-a** was significantly higher (∼4.0%) than **Control-a**, suggesting that the increased magnetism is likely due to the properties of the coating rather than through any variation in chip mass. The inverse spin Hall effect (E_{ISHE}) is a key factor for electric current generation in LSSE devices, where the in-plane surface magnetization ($M^{\parallel}_{sur}$) is directly proportional to inverse spin Hall effect ($E_{ISHE} \propto \nabla T \times M^{\parallel}_{sur}$). None of our samples exhibited magnetic hysteresis, indicating that these YIG/GGG chips had only weak magnetic coercivity at low fields (≤0.5 mT). As the applied magnetic field was further increased, the induced sample magnetization increased very slowly due to paramagnetism.

To understand the surface magnetization effects in sample **BSYIG1-a** further, magnetic force microscope (MFM) measurements were undertaken (Park SYSTEMS NX7 instrument using a Nanoworld MFMR probe). MFM differs from traditional atomic force microscopy in that the probe, in addition to providing a surface height profile, is also able to detect the magnetic field gradient above the sample. MFM surface profiling of **BSYIG1-a** revealed that a typical ribbon is comprised of multilayers of Bi_2Se_3, providing thicker sections ca. 250 nm thick [e.g., the profile along vector **1** in Figs. 3(a) and 3(b)] and additional thinner sections ca. 100 nm thick [e.g., the profile along vector **2** in Figs. 3(a) and 3(b)]. Re-running ribbon profiles **1** and **2** with the magnetic probe at a height of 100 nm above the topological surface provided data on the magnetic field gradient variation along the same line profiles. The MFM amplitude [Figs. 3(c) and 3(d)] increases over the Bi_2Se_3 flake, and furthermore, the magnetic enhancement correlates with the thickness of the Bi_2Se_3, being larger for the thicker part of the sample. This amplitude enhancement suggests that the observed effect is magnetic rather than due to long-range electrostatics, supporting the inference that the surface magnetization is improved by the

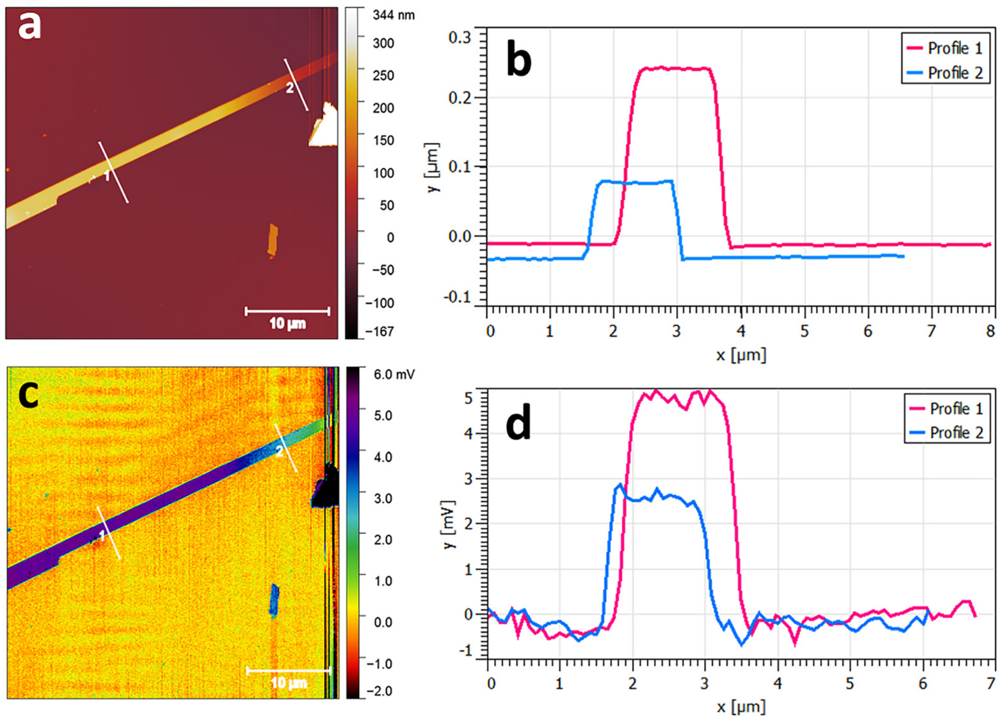

FIG. 3. Scanning probe microscopy images of **BSYIG1-a**: (a) Atomic force microscopy image of a representative Bi_2Se_3 nanoribbon on a YIG/GGG substrate. (b) Bi_2Se_3 ribbon profile scans along vectors **1** (pink) and **2** (blue) showing the two differential height responses. (c) Magnetic force microscopy image of the same Bi_2Se_3 nanoribbon. The measurement was performed at 100 nm above the topological heights determined in the AFM study. (d) MFM profile scans along vectors **1** (pink) and **2** (blue) showing the magnetic response.

presence of Bi_2Se_3 flakes at the interlayer of a Pt/YIG device. However, it was not possible to extract quantitative information about surface magnetization from this study, but we are hopeful that future experimental and theoretical work can provide further explanation.

In conclusion, Bi_2Se_3 nanoribbons provide a significant improvement in Pt/YIG spin Seebeck voltages at low surface coverages (2.5%). Spin Seebeck coefficients in the range of 0.34–0.62 μV/K for Pt/Bi_2Se_3/YIG are attained for our measured devices, compared to just 0.09 μV/K for Pt/YIG controls alone, for a 12 K thermal gradient and a magnetic field swept from -50 to $+50$ mT. SQUID and MFM measurements provide evidence that surface magnetism concentration by the Bi_2Se_3 nanoribbons is an important feature associated with SSE enhancement. These results provide interesting avenues for further experimentation and will hopefully stimulate theoretical debate and development in the longitudinal spin Seebeck field.

See the supplementary material for further details of instrumentation, sample preparation, the spin Seebeck measurement setup, SEM, EDX, SQUID, the effects of YIG cleaning procedures, and further details of data reduction, reproducibility, and errors across all samples measured.

This work was supported by the Engineering and Physical Sciences Research Council (EPSRC) under Grant No. EP/V047256/1 and by the University of Nottingham Propulsion Futures Beacon. M.P.W. acknowledges funding from a Nottingham Research Fellowship aligned to the Beacon. We thank the referees of this paper for their valuable insights and comments.

AUTHOR DECLARATIONS

Conflict of Interest

The authors have no conflicts to disclose.

Author Contributions

Yaoyang Hu: Conceptualization (equal); Data curation (equal); Formal analysis (equal); Funding acquisition (equal); Investigation (equal); Methodology (equal); Project administration (equal); Software (equal); Supervision (equal); Validation (equal); Visualization (equal); Writing – original draft (equal); Writing – review & editing (equal). **Vladimir Korolkov:** Formal analysis (equal); Investigation (equal); Methodology (equal); Writing – review & editing (equal). **James Kertfoot:** Formal analysis (equal); Investigation (equal); Methodology (equal); Writing – review & editing (equal). **Oleg Makarovsky:** Conceptualization (equal); Formal analysis (equal); Funding acquisition (equal); Investigation (equal); Methodology (equal); Project administration (equal); Resources (equal); Supervision (equal); Validation (equal); Visualization (equal); Writing – original draft (equal); Writing – review & editing (equal). **Simon Woodward:** Conceptualization (equal); Formal analysis (equal); Funding acquisition (equal); Investigation (equal); Methodology (equal); Project administration (equal); Resources (equal); Supervision (equal); Validation (equal); Visualization (equal); Writing – original draft (equal); Writing – review & editing (equal). **Michael Peter Weir:** Conceptualization (equal); Data curation (equal); Formal analysis (equal); Funding acquisition (equal); Investigation (equal); Methodology (equal);

Project administration (equal); Software (equal); Supervision (equal); Validation (equal); Visualization (equal); Writing – original draft (equal); Writing – review & editing (equal). **H. Jessica Pereira:** Investigation (equal); Methodology (equal); Validation (equal); Writing – review & editing (equal). **Oliver James Amin:** Formal analysis (equal); Investigation (equal); Methodology (equal). **Jem Pitcairn:** Formal analysis (equal); Investigation (equal); Methodology (equal). **Matthew J. Cliffe:** Formal analysis (equal); Investigation (equal); Methodology (equal); Writing – review & editing (equal). **A. W. Rushforth:** Formal analysis (equal); Investigation (equal); Methodology (equal); Validation (equal); Writing – review & editing (equal). **Gunta Kunakova:** Conceptualization (equal); Formal analysis (equal); Investigation (equal); Methodology (equal); Writing – original draft (equal); Writing – review & editing (equal). **Kiryl Niherysh:** Formal analysis (equal); Investigation (equal); Methodology (equal); Writing – review & editing (equal).

DATA AVAILABILITY

The data that support the findings of this study are available from the supplementary material or the corresponding authors upon reasonable request.

REFERENCES

[1]T. Kikkawa and E. Saitoh, Annu. Rev. Condens. Matter Phys. **14**, 129–151 (2023).
[2]N. Nandihalli, Mater. Today Energy **25**, 100965 (2022).
[3]S. S. Costa and L. C. Sampaio, J. Magn. Magn. Mater. **547**, 168773 (2022).
[4]J. Holanda, O. Alves Santos, R. O. Cunha, J. B. S. Mendes, R. L. Rodríguez-Suárez, A. Azevedo, and S. M. Rezende, Phys. Rev. B **95**(21), 214421 (2017).
[5]M. Gamino, J. G. S. Santos, A. L. R. Souza, A. S. Melo, R. D. Della Pace, E. F. Silva, A. B. Oliveira, R. L. Rodríguez-Suárez, F. Bohn, and M. A. Correa, J. Magn. Magn. Mater. **527**, 167778 (2021).
[6]K. Ando, S. Takahashi, J. Ieda, Y. Kajiwara, H. Nakayama, T. Yoshino, K. Harii, Y. Fujikawa, M. Matsuo, S. Maekawa, and E. Saitoh, J. Appl. Phys. **109**(10), 103913 (2011).
[7]K. Uchida, J. Xiao, H. Adachi, J. Ohe, S. Takahashi, J. Ieda, T. Ota, Y. Kajiwara, H. Umezawa, H. Kawai, G. E. W. Bauer, S. Maekawa, and E. Saitoh, Nat. Mater. **9**, 894–897 (2010).
[8]Z. Qiu, K. Ando, K. Uchida, Y. Kajiwara, R. Takahashi, H. Nakayama, T. An, Y. Fujikawa, and E. Saitoh, Appl. Phys. Lett. **103**(9), 092404 (2013).
[9]X. Jia, K. Liu, K. Xia, and G. E. W. Bauer, Europhys. Lett. **96**(1), 17005 (2011).
[10]A. Kirihara, K. I. Uchida, Y. Kajiwara, M. Ishida, Y. Nakamura, T. Manako, E. Saitoh, and S. Yorozu, Nat. Mater. **11**(8), 686–689 (2012).
[11]H. Yuasa, K. Tamae, and N. Onizuka, AIP Adv. **7**(5), 055928 (2017).
[12]H. Yuasa, F. Nakata, R. Nakamura, and Y. Kurokawa, J. Phys. D: Appl. Phys. **51**(13), 134002 (2018).
[13]J. Cramer, U. Ritzmann, B. W. Dong, S. Jaiswal, Z. Qiu, E. Saitoh, U. Nowak, and M. Kläui, J. Phys. D: Appl. Phys. **51**(14), 144004 (2018).
[14]F. Nakata, T. Niimura, Y. Kurokawa, and H. Yuasa, Jpn. J. Appl. Phys., Part 1 **58**, 090602 (2019).
[15]T. Niimura, Y. Kurokawa, S. Horiike, H. Li, H. Hanamoto, R. Weber, A. Berger, and H. Yuasa, Phys. Rev. B **102**(9), 094411 (2020).
[16]M. Schreier, N. Roschewsky, E. Dobler, S. Meyer, H. Huebl, R. Gross, and S. T. B. Goennenwein, Appl. Phys. Lett. **103**(24), 242404 (2013).
[17]H. Wang, C. Du, P. C. Hammel, and F. Yang, Phys. Rev. Lett. **113**(9), 97202 (2014).
[18]V. Kalappattil, R. Geng, R. Das, M. Pham, H. Luong, T. Nguyen, A. Popescu, L. M. Woods, M. Kläui, H. Srikanth, and M. H. Phan, Mater. Horiz. **7**(5), 1413–1420 (2020).
[19]W. Y. Lee, M. S. Kang, G. S. Kim, N. W. Park, K. Y. Choi, C. T. Le, M. U. Rashid, E. Saitoh, Y. S. Kim, and S. K. Lee, ACS Appl. Mater. Interfaces **13**(13), 15783–15790 (2021).
[20]S. K. Lee, W. Y. Lee, T. Kikkawa, C. T. Le, M. S. Kang, G. S. Kim, A. D. Nguyen, Y. S. Kim, N. W. Park, and E. Saitoh, Adv. Funct. Mater. **30**(35), 2003192 (2020).
[21]W. Y. Lee, N. W. Park, M. S. Kang, G. S. Kim, H. W. Jang, E. Saitoh, and S. K. Lee, J. Phys. Chem. Lett. **11**(13), 5338–5344 (2020).
[22]W. Lin, K. Chen, S. Zhang, and C. L. Chien, Phys. Rev. Lett. **116**(18), 186601 (2016).
[23]A. Prakash, J. Brangham, F. Yang, and J. P. Heremans, Phys. Rev. B **94**(1), 014427 (2016).
[24]D. Kikuchi, M. Ishida, K. Uchida, Z. Qiu, T. Murakami, and E. Saitoh, Appl. Phys. Lett. **106**(8), 82401 (2015).
[25]Y. Saiga, K. Mizunuma, Y. Kono, J. C. Ryu, H. Ono, M. Kohda, and E. Okuno, Appl. Phys. Express **7**(9), 093001 (2014).
[26]J. Andzane, G. Kunakova, S. Charpentier, V. Hrkac, L. Kienle, M. Baitimirova, T. Bauch, F. Lombardi, and D. Erts, Nanoscale **7**(38), 15935–15944 (2015).
[27]See https://imagej.nih.gov/ij/ for further documentation on the ImageJ software and installation instructions, accessed 15 April 2023.
[28]D. Kong, J. J. Cha, K. Lai, H. Peng, J. G. Analytis, S. Meister, Y. Chen, H. J. Zhang, I. R. Fisher, Z. X. Shen, and Y. Cui, ACS Nano **5**(6), 4698–4703 (2011).